Nucleon charge and magnetisation distributions: flavour separation and zeroes

Zhao-Qian Yao [ID],[1, 2, 3] Daniele Binosi [ID],[3] Zhu-Fang Cui[ID],[1, 2] and Craig D. Roberts[ID,1, 2]

[1]*School of Physics, Nanjing University, Nanjing, Jiangsu 210093, China*
[2]*Institute for Nonperturbative Physics, Nanjing University, Nanjing, Jiangsu 210093, China*
[3]*European Centre for Theoretical Studies in Nuclear Physics and Related Areas,*
Villa Tambosi, Strada delle Tabarelle 286, I-38123 Villazzano (TN), Italy
(Dated: 2024 March 12)
Email: zyao@ectstar.eu (ZQY); binosi@ectstar.eu (DB); phycui@nju.edu.cn (ZFC); cdroberts@nju.edu.cn (CDR)

A symmetry-preserving truncation of the quantum field equations describing hadron properties is used to deliver parameter-free predictions for all nucleon elastic electromagnetic form factors and their flavour separation to large values of momentum transfer, Q^2. The proton electric form factor, G_E^p, possesses a zero, whereas that of the neutron, G_E^n, does not. The difference owes to the behaviour of the Pauli form factor of the proton's singly-represented valence d-quark. Consequently, $G_E^n > G_E^p$ on a material large-Q^2 domain. These predictions can be tested in modern experiments.

1. Introduction — The proton is Nature's most fundamental bound state. It is supposed to be described by quantum chromodynamics (QCD), which is the Poincaré-invariant quantum non-Abelian gauge field theory that describes strong interactions within the Standard Model. The QCD Lagrangian density is expressed in terms of gluon and quark partons (and ghosts, too, in many gauges) [1]. In these terms, the proton consists of three valence-quark partons $(u + u + d)$ and infinitely many gluon and sea-quark partons – see Fig. 1. If science is to claim an understanding of Nature, then it must deliver a sound description of proton properties from QCD; not just its mass, but also its entire array of structural properties [2–7].

The proton bound-state problem can be addressed in any approach that provides access to the three-quark six-point Schwinger function [8, 9]. Lattice-regularised QCD (lQCD) provides one such framework [10]. Modern applications are sketched in Ref. [11, Sec. 10]. Continuum Schwinger function methods (CSMs) provide another widely used approach to nucleon (proton, p, and neutron, n) structure [12–16]. Many such studies use

a quark + dynamical diquark picture of the nucleon because it vastly simplifies the problem [17]. Notwithstanding that, the approximations implicit in the simplification need checking and tighter links must be forged with QCD. These things can be accomplished by beginning with an explicitly symmetry-preserving truncation of all quantum field equations (Dyson-Schwinger equations – DSEs) relating to the nucleon bound-state problem. The first studies of this type were reported in Refs. [18, 19].

A highlight of proton structure studies this century is the collection of data that hints at the existence of a zero in the proton elastic electric form factor [20–25]. This is complemented by the discovery of marked differences in the charge and magnetisation distributions of different valence-quark flavours (u vs. d) within the proton [26, 27]. Modern and foreseen facilities will both obtain data that can check existing measurements and push empirical knowledge of all nucleon form factors to momentum transfers $Q^2 > 10 \, \text{GeV}^2$ [27, 28]. This prospect challenges theory to deliver predictions for all such form factors that extend far onto this domain in frameworks with a traceable connection to QCD.

Herein, we approach this challenge by using a symmetry-preserving leading-order (rainbow-ladder – RL) truncation of all DSEs needed to calculate the seven-point Schwinger function that defines the matrix element from which nucleon elastic electromagnetic form factors can be extracted [29, 30]. Existing algorithms have limited the reach of such form factor calculations to $Q^2 \lesssim 4 \, \text{GeV}^2$. We extend the results to $Q^2 \gtrsim 12 \, \text{GeV}^2$ using the statistical Schlessinger point method (SPM) [31–36], which may also be called a statistical multi-point Padé approximant scheme. The SPM is grounded in analytic function theory. It is free from practitioner-induced bias; hence, delivers objective analytic continuations.
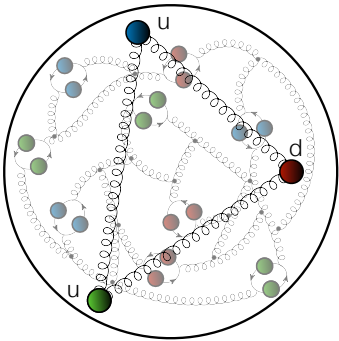

FIG. 1. Proton: two valence up (u) quark partons, one valence down (d) quark parton, and infinitely many gluon and sea-quark partons, drawn here as "springs" and closed loops, respectively. The neutron is the proton's isospin partner, two d quark partons, one u quark parton, and glue and sea.

2. Nucleon bound state — The RL truncation nucleon Faddeev equation is drawn in Fig. 2. Discussions of the formulation and solution of this linear, homogeneous integral equation are provided, *e.g.*, in Refs. [37–39]. The key element is the quark+quark scattering kernel, for
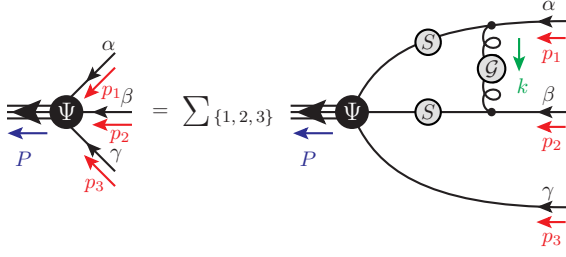
FIG. 2. Faddeev equation. Filled circle: Faddeev amplitude, Ψ, the matrix-valued solution, which involves 128 independent scalar functions. Spring: dressed-gluon interaction that mediates quark+quark scattering, Eqs. (1), (2). Solid line: dressed-quark propagator, S, calculated from the rainbow gap equation. Lines not adorned with a shaded circle are amputated. Isospin symmetry is assumed.

which the RL truncation is obtained by writing [40]:

$$\mathcal{K}_{tu}^{rs}(k) = \mathcal{G}_{\mu\nu}(k)[i\gamma_\mu \frac{\lambda^a}{2}]_{ts}[i\gamma_\nu \frac{\lambda^a}{2}]_{ur}, \qquad (1a)$$

$$\mathcal{G}_{\mu\nu}(k) = \tilde{\mathcal{G}}(y)T_{\mu\nu}(k), \qquad (1b)$$

$k^2 T_{\mu\nu}(k) = k^2 \delta_{\mu\nu} - k_\mu k_\nu$, $y = k^2$. The tensor structure specifies Landau gauge, used because it is a fixed point of the renormalisation group and that gauge for which corrections to RL truncation are least significant [41]. In Eq. (1), r, s, t, u represent colour, spinor, and flavour matrix indices (as necessary).

A realistic form of $\mathcal{G}_{\mu\nu}(y)$ is explained in Refs. [44, 45]:

$$\tilde{\mathcal{G}}(y) = \frac{8\pi^2}{\omega^4} D e^{-y/\omega^2} + \frac{8\pi^2 \gamma_m \mathcal{F}(y)}{\ln\left[\tau + (1 + y/\Lambda_{\mathrm{QCD}}^2)^2\right]}, \qquad (2)$$

where $\gamma_m = 12/25$, $\Lambda_{\mathrm{QCD}} = 0.234\,\mathrm{GeV}$, $\tau = \mathrm{e}^2 - 1$, and $\mathcal{F}(y) = \{1 - \exp(-y/\Lambda_I^2)\}/y$, $\Lambda_I = 1\,\mathrm{GeV}$. We employ a mass-independent (chiral-limit) momentum-subtraction renormalisation scheme [46].

Widespread use has shown [15] that interactions in the class containing Eqs. (1), (2) can serve to unify the properties of many systems. Contemporary studies employ $\omega = 0.8\,\mathrm{GeV}$ [47, 48]. Then, with $\omega D = 0.8\,\mathrm{GeV}^3$ and renormalisation point invariant quark current mass $\hat{m}_u = \hat{m}_d = 6.04\,\mathrm{MeV}$, which corresponds to a one-loop mass at $\zeta = 2\,\mathrm{GeV}$ of $4.19\,\mathrm{MeV}$, the following predictions are obtained: pion mass $m_\pi = 0.14\,\mathrm{GeV}$; nucleon mass $m_N = 0.94\,\mathrm{GeV}$; and pion leptonic decay constant $f_\pi = 0.094\,\mathrm{GeV}$. These values align with experiment [49]. (See also Eq. (8) – supplementary material.) When the product ωD is kept fixed, physical observables remain practically unchanged under $\omega \to (1 \pm 0.2)\omega$ [50].

All subsequent calculations are parameter-free. The interaction involves one parameter and there is a single quark current-mass. Both quantities are now fixed.

3. Nucleon electromagnetic current — Working with the solution of the Faddeev equation in Fig. 2, the interaction current drawn in Fig. 3 is necessary and sufficient

to deliver a photon+nucleon interaction that is consistent with all relevant Ward-Green-Takahashi identities; hence, *inter alia*, ensures electromagnetic current conservation. The current can be written as follows ($N = p, n$):

$$J_\mu^N(Q) = ie\Lambda_+(p_f)[F_1^N(Q^2)\gamma_\mu$$
$$+ \frac{1}{2m_N}\sigma_{\mu\nu}Q_\nu F_2^N(Q^2)]\Lambda_+(p_i) \qquad (3)$$

where e is the positron charge, the incoming and outgoing nucleon momenta are $p_{i,f}$, $Q = p_f - p_i$, $\Lambda_+(p_{i,f})$ are positive-energy nucleon-spinor projection operators, and $F_{1,2}^N$ are the Dirac and Pauli form factors. The charge and magnetisation distributions are ($\tau = Q^2/[4m_N^2]$) [51]:

$$G_E^N = F_1^N - \tau F_2^N, \quad G_M^N = F_1^N + F_2^N. \qquad (4)$$

Numerical methods for solving sets of coupled gap, Bethe-Salpeter, and Faddeev equations are described, *e.g.*, in Refs. [37, 40, 52, 53]. Exploiting these schemes, we solved all equations relevant to calculation of the current in Eq. (3) and computed the current itself, thereby arriving at predictions for the form factors in Eq. (4).

A technical remark is appropriate here. The Faddeev equation solution depends on two relative momenta, p, q, and the nucleon total momentum, P. This leads to a dependence on three angular variables defined via the inner products $p \cdot q$, $p \cdot P$, $q \cdot P$. In solving the equation, eight Chebyshev polynomials are used to express the dependence on each angle [40]. This enables evaluation of Ψ at any required integration point in either the Faddeev equation or the current. P is a complex-valued (timelike) vector, $P^2 = -m_N^2$, whereas Q is spacelike. So, when evaluating the current, the integrand sample points are typically in the complex plane. This entails oscillations whose amplitudes grow with Q^2 [54]. Increasing the number of Chebyshev polynomials and quadrature points is effective on $Q^2 \lesssim 4\,\mathrm{GeV}^2$. At larger Q^2 values, however, this brute force approach fails to deliver accurate results.

In order to obtain predictions on $Q^2 \gtrsim 4\,\mathrm{GeV}^2$, we extrapolate using the SPM, whose properties and accuracy are explained elsewhere [31–36]. The SPM is based on the Padé approximant. It accurately reconstructs a function in the complex plane within a radius of convergence determined by that one of the function's branch points which lies closest to the real domain that provides the sample points. Modern implementations introduce a statistical element; so, the extrapolations come with an objective and reliable estimate of uncertainty.

4. Nucleon form factors — Our predictions for nucleon static properties are collected in Table I. In magnitude, the magnetic moments are $\sim 25\%$ too small. This is a failing of RL truncation, which produces a photon+quark vertex whose dressed-quark anomalous magnetic moment term is too weak. It is corrected in higher-order truncations [55, 56]. Such corrections have been implemented in studies of mesons [47]. It may be possible to adapt this approach to baryons. Concerning the other entries in Table I, the agreement with experiment is reasonable.
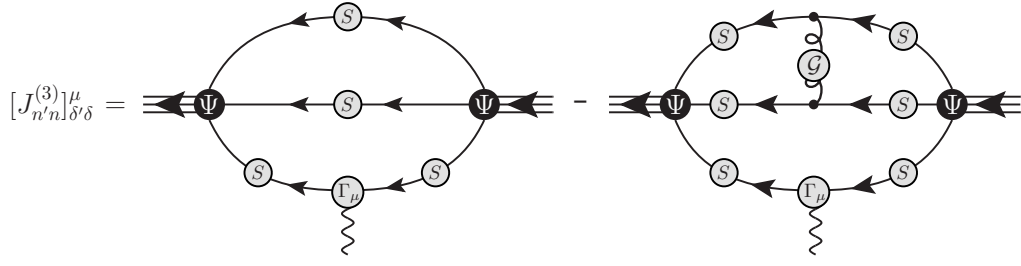
FIG. 3. $a = 3$ spinor component of the nucleon electromagnetic current. δ, δ' are spinor indices and n, n' are isospin indices. Γ_μ is the dressed-photon+quark vertex, which can be obtained, $e.g.$, following Ref. [42]. As explained elsewhere [43, Appendix B], the complete current has three terms: $J_\mu(Q) = \sum_{a=1,2,3} J_\mu^a(Q)$; but using symmetries, one can readily obtain the $a = 1, 2$ components of the current once $a = 3$ is known.

Faddeev equation predictions for each nucleon form factor agree well with data [59–73]. (See Figs. 6, 7 – supplementary material for confirmation.) Even $G_E^n(Q^2)$, which is difficult to explain because of its sensitivity to details of the neutron wave function, especially as expressed in F_1^n – see, $e.g.$, Refs. [12, 74]. Notably, $G_M^{p,n}(Q^2)/\mu_{p,n}$ agree well with experiment.

The last point is important in connection with the prediction for $\mu_p G_E^p(Q^2)/G_M^p(Q^2)$ drawn in Fig. 4A. Directly calculated Faddeev equation results are available on $Q^2 \lesssim 4 \, \text{GeV}^2$. Thereafter, we calculate two sets of SPM results: (I) ratio formed from curves obtained via independent SPM analyses of $G_{E,M}^p$; (II) SPM analysis of the ratio $\mu_p G_E^p/G_M^p$ obtained on the directly accessible domain. (A quantitative explanation of the SPM characteristics is provided in the supplementary material.) Both methods yield compatible results and agree with all available data within mutual uncertainties. Significantly, a zero is predicted in G_E^p:

$$\text{SPM I:} \quad Q^2_{G_E^p - \text{zero}} = 8.37^{+1.68}_{-0.81} \, \text{GeV}^2 \,, \quad (5a)$$

$$\text{SPM II:} \quad Q^2_{G_E^p - \text{zero}} = 9.59^{+2.09}_{-0.85} \, \text{GeV}^2 \,. \quad (5b)$$

Being compatible, they can be averaged, with the result: $Q^2_{G_E^p - \text{zero}} = 8.86^{+1.93}_{-0.86} \, \text{GeV}^2$.

TABLE I. Static properties: magnetic moments in nuclear magnetons and radii-squared in fm^2, calculated using conventional definitions – Eq. (9) – supplementary material. Empirical values from Ref. [49, PDG]. The column "SPM" lists radii extracted from experimental data using the SPM [57, 58].

	herein	Exp.	SPM
μ_p	2.23	2.793	
μ_n	-1.33	-1.913	
$\langle r_E^2 \rangle^p$	0.788	0.7070(7)	0.717(14)
$\langle r_E^2 \rangle^n$	-0.0621	$-0.1160(22)$	
$\langle r_M^2 \rangle^p$	0.672	0.72(4)	0.667(44)
$\langle r_M^2 \rangle^n$	0.661	0.75(2)	

Notably, as suggested elsewhere [75, 76], we have confirmed that if the quark+quark interaction is modified such that dressed quarks more rapidly become parton like, then $Q^2_{G_E^p - \text{zero}}$ is shifted to a larger value. The location of the zero in G_E^p is thus confirmed to be a sensitive expression of gauge sector dynamics and emergent hadron mass [14–16].

We depict the Faddeev equation prediction for $\mu_n G_E^n(Q^2)/G_M^n(Q^2)$ in Fig. 4B. The agreement with data is fair and the trend is correct. Given that our prediction delivers a good description of $G_M^n(Q^2)/\mu_n$, the quantitative mismatch owes to the imperfect description of G_E^n – see Eq. (11) – supplementary material. No signal is found for a zero in $\mu_n G_E^n(Q^2)/G_M^n(Q^2)$. It follows that there is a Q^2 domain upon which the charge form factor of the neutral neutron is larger than that of the positively charged proton. It begins at $Q^2 = 4.66^{+0.18}_{-0.13} \, \text{GeV}^2$.

At first glance, the absence of a zero in $\mu_n G_E^n(Q^2)/G_M^n(Q^2)$ conflicts with the other existing Poincaré-invariant study of nucleon form factors at large Q^2, which employs a quark+diquark approach [78]. However, that study locates the zero at $Q^2_{G_E^n - \text{zero}} = 20.1^{+10.6}_{-3.5} \, \text{GeV}^2$, $i.e.$, an uncertain location beyond the range of foreseeable measurements. Looking closer, the predictions herein and those in Ref. [78] are largely in semiquantitative agreement. Apparently minor differences, however, are amplified at large Q^2.

Supposing one can neglect strange quark contributions to nucleon form factors, which is a good approximation [79], then a flavour separation is possible using the following identities: $F_i^u = 2F_i^p + F_i^n$, $F_i^d = F_i^p + 2F_i^n$, $i = 1, 2$. Current conservation and valence-quark number entail $F_1^u(Q^2 = 0) = 2$, $F_1^d(Q^2 = 0) = 1$.

Our parameter-free predictions for these form factors are drawn in Fig. 5. They deliver good qualitative and fair quantitative agreement with available data. A zero is projected in F_1^d at

$$Q^2_{F_1^d - \text{zero}} = 5.73^{+1.46}_{-0.49} \, \text{GeV}^2. \quad (6)$$

This matches the result obtained in the quark+diquark picture [78]: $Q^2 = 7.0^{+1.1}_{-0.4} \, \text{GeV}^2$. No signal is found for a zero in any other form factor in Fig. 5. The
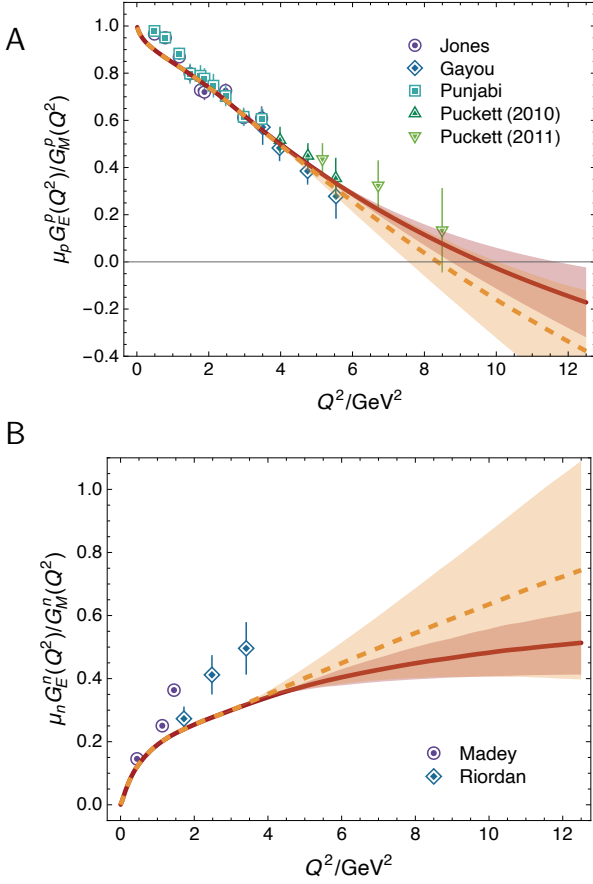
FIG. 4. Panel A: $\mu_p G_E^p/G_M^p$. Panel B: $\mu_n G_E^n/G_M^n$. SPM I – dashed orange curve within like-coloured band; and SPM II – solid red curve within like-coloured band. Data: proton – Refs. [20–24]; and neutron – Refs. [68, 77].

FIG. 5. Flavour separation: $Q^2 F_1^{d,u}$ (Panel A); and $Q^2 F_2^{d,u}$ (Panel B). Data: Ref. [26].

quark+diquark picture produces an uncertain zero in F_2^d at very large momentum transfer: $Q^2 = 12.0_{-1.7}^{+3.9}\,\text{GeV}^2$.

As explained elsewhere [74], in the isospin symmetry limit, the behaviours of $\mu_p G_E^p(Q^2)/G_M^p(Q^2)$ and $\mu_n G_E^n(Q^2)/G_M^n(Q^2)$ are not independent. This is readily seen by exploiting isospin symmetry in writing a flavour separation of the charge and magnetisation form factors ($e_u = 2/3$, $e_d = -1/3$):

$$G_E^p = e_u G_E^{pu} + e_d G_E^{pd}, \quad G_E^n = e_u G_E^{pd} + e_d G_E^{pu}. \quad (7)$$

Regarding these identities, we note that G_E^p possesses a zero because, although remaining positive, G_E^{pu}/G_M^p falls steadily with increasing Q^2 whereas G_E^{pd}/G_M^p is positive and approximately constant. On the other hand and consequently, G_E^n does not exhibit a zero because $e_u > 0$, G_E^{pd}/G_M^p is large and positive, and $|e_d G_E^{pu}|$ is always less than $e_u G_E^{pd}$. These arguments are supported by Fig. 8 – supplementary material.

The character of G_E^{pd}/G_M^p owes to the fact that F_2^d is negative definite on the entire domain displayed in Fig. 5 and $G_E^d = F_1^d - (Q^2/[4m_N]^2)F_2^d$, whereas F_1^d falls toward its zero. This is not the case for the quark+diquark cal-
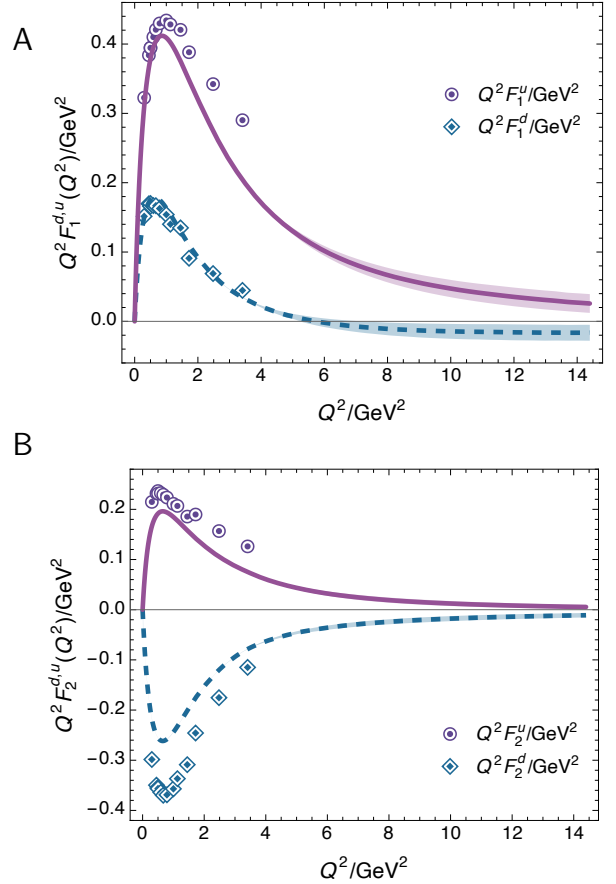
culation, in which F_2^d also exhibits a zero; so, at some Q^2, G_E^{pd} begins to diminish in magnitude – see, e.g., Ref. [80, Fig. 7.3]. Plainly, the larger Q^2 behaviour of F_2^d is key to the existence/absence of a zero in G_E^n.

Notwithstanding these differences, it is clear that, as in the quark+diquark picture [78], if the zero in G_E^p/G_M^p moves to larger Q^2, then G_E^n/G_M^n exhibits slower growth on $Q^2 \gtrsim Q^2_{F_1^d-\text{zero}}$. This correlation is also consistent with results obtained using lQCD [81].

5. Summary and Perspectives — Using a symmetry-preserving truncation of the quantum field equations relevant to calculation of hadron masses and interactions, this study delivers parameter-free predictions for all nucleon charge and magnetisation distributions and their flavour separation. Each element in this analysis possesses an unambiguous link with analogous quantities in quantum chromodynamics (QCD) and the study unifies nucleon properties with those of numerous other hadrons – see, e.g., Refs. [15, 82, 83]. These features provide support for the reliability of the results herein.

The proton electric form factor, $G_E^p(Q^2)$, is predicted to possess a zero at a Q^2 location within reach of modern experiments. On the other hand, the neutron electric form factor, G_E^n, does not exhibit a zero. Conse-
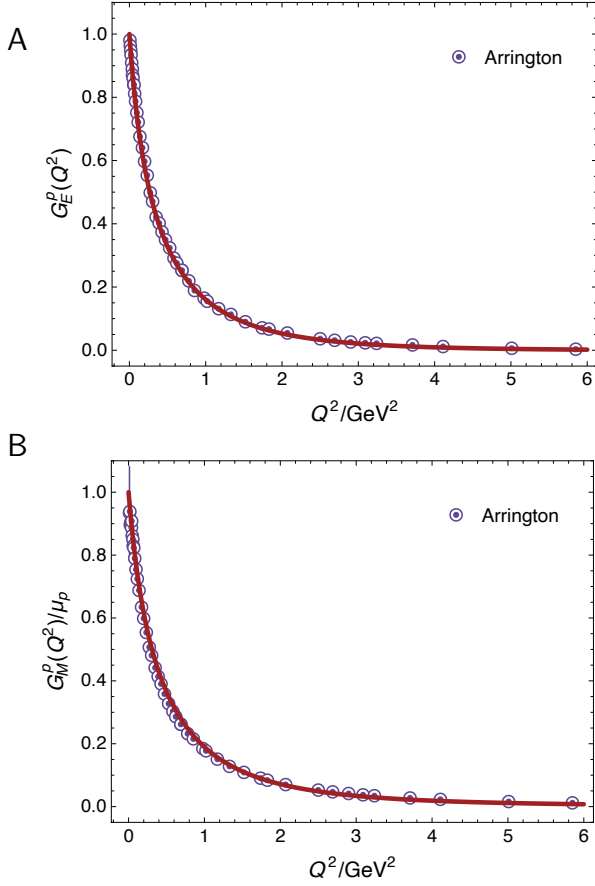
FIG. 6. Proton electromagnetic form factors: solid red line – results obtained herein. Experimental data taken from compilation in Ref. [59].
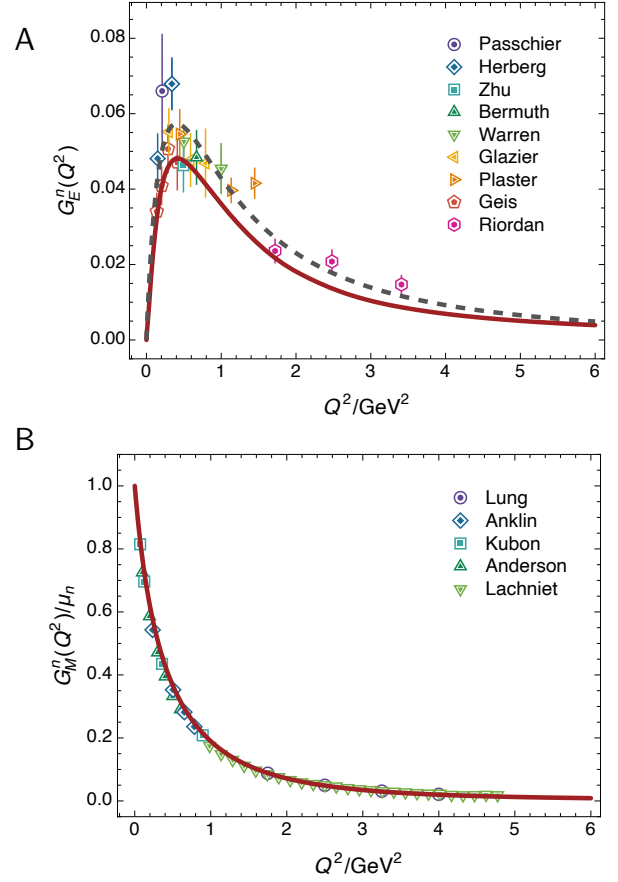

FIG. 7. Neutron electromagnetic form factors. Solid red curve – results obtained herein. Dashed black curve in panel A – Ref. [84, Kelly] parametrisation of data. G_E^n experimental data: Refs. [60–68]. G_M^n data: Refs. [69–73]

quently, anticipated experiments will see $|G_E^n/G_E^p| > 1$. These outcomes rest with the behaviour of the proton's d-quark Pauli form factor and all are sensitive expressions of emergent phenomena in QCD.

No material improvement of the analysis herein can be anticipated before a way is found to include higher-order truncations in the continuum baryon bound-state problem or lattice-regularised QCD produces precise results on a similar domain to that discussed herein. Meanwhile, the framework used herein can be applied to other high-profile challenges [2–7], *e.g.*, prediction of baryon electroweak form factors, nucleon-to-resonance transition form factors, and nucleon gravitational form factors.

.... *Supplementary Material* ....

This material is included to demonstrate that our parameter-free predictions for individual charge and magnetisation form factors are in good agreement with available data; and illustrate, exemplify and/or support some other remarks in the main text.

Following Ref. [44], one may draw a connection between the interaction in Eq. (2) and QCD's process-independent effective charge, discussed in Refs. [85, 86]. That effective charge is characterised by an infrared coupling value $\hat{\alpha}(0)/\pi = 0.97(4)$ and a gluon mass-scale $\hat{m}_0 = 0.43(1)\,\text{GeV}$. The following values are those of analogous quantities inferred from Eq. (2):

$$\alpha_{\mathcal{G}}(0)/\pi = 1.45\,, \quad m_{\mathcal{G}} = 0.54\,\text{GeV}\,. \tag{8}$$

They compare tolerably well with the QCD values, especially if one recalls that earlier versions of the RL interaction yielded $\alpha_{\mathcal{G}}(0)/\pi \approx 15$, *i.e.*, a value ten-times larger [44].

The quantities in Table I were calculated using stan-

dard definitions: $\mu_N = G_M^N(Q^2 = 0)$;

$$\langle r_F^2 \rangle^N = -6 \frac{d \ln G_F^N(Q^2)}{dQ^2}\bigg|_{Q^2=0}, \quad (9)$$

$F = E$, M, except $\langle r_E^2 \rangle^n = -6G_E^{n\prime}(Q^2)|_{Q^2=0}$ because $G_E^n(0) = 0$. It is worth highlighting the prediction $\langle r_E^2 \rangle^p > \langle r_M^2 \rangle^p$, which accords with SPM analyses of existing form factor data [57, 58]. This ordering of radii is responsible for the decay of $\mu_p G_E^p / G_M^p$ away from unity on $Q^2 \simeq 0$ that is apparent in Fig. 4A.

Our SPM extrapolations are developed as follows.

Step 1: For each function considered, we produce $N = 40$ directly calculated function values spaced evenly on $Q^2 \lesssim 4\,\text{GeV}^2$.

Step 2: From that set, $M_0 = 14$ points are chosen at random, the usual SPM continued fraction interpolation is constructed, and that function is extrapolated onto $Q^2/\text{GeV}^2 \in [4, 12]$. The curve is retained so long as it is singularity free.

Step 3: This is repeated with another set of M_0 randomly chosen points. Steps 2 and 3 admit $\approx 5 \times 10^{10}$ independent extrapolations.

Step 4: One continues with 2 and 3 until $n_{M_0} = 500$ smooth extrapolations are obtained.

Step 5: Steps 2 and 3 are repeated for $M = \{M_0 + 2i | i = 1, \ldots, 6\}$

Step 6: At this point, one has 3 000 statistically independent extrapolations.

Working with these extrapolations, then at each value of Q^2, we record the mean value of all curves as the central prediction and report as the uncertainty the function range which contains 68% of all the extrapolations – this is a 1σ band.

It is worth comparing the predictions in Figs. 6, 7 with the parametrisations of data provided in Ref. [84, Kelly]. A useful quantitative measure is the relative $\mathcal{L}_1$ differ-

ence: $\Delta_F^N = 2[\delta_-]_F^N / [\delta_+]_F^N$, where

$$[\delta_\mp]_F^N = \int_0^{10\,\text{GeV}^2} dQ^2$$
$$|\text{Prediction}_F^N(Q^2) \mp \text{Kelly}_F^N(Q^2)|. \quad (10)$$

The upper bound is that employed practically in Ref. [84]. The results are:

$$\begin{array}{c|c|c|c|c} & G_E^p & G_M^p & G_E^n & G_M^n \\ \hline \Delta_F^N (\%) & 4.9 & 7.2 & 21 & 4.0 \end{array} \quad (11)$$

Evidently, the parameter-free Faddeev equation predictions are practically indistinguishable from the data fits [84], except in the case of G_E^n, which, in the mean, lies systematically below the data by $\approx 20\%$. These features
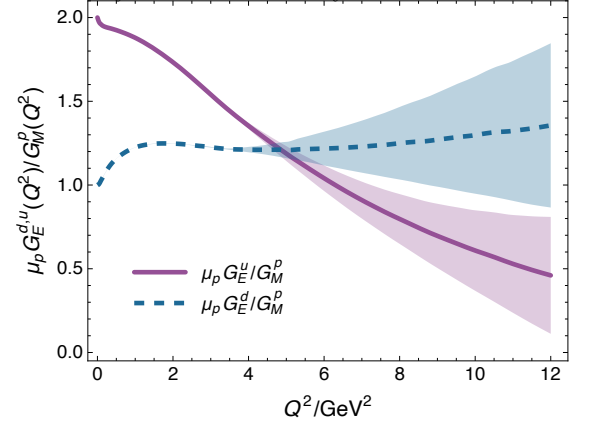

FIG. 8. Flavour separation of the charge and magnetisation form factors, with each function normalised by G_M^p in order to highlight their differing Q^2-dependence.

are also illustrated in Figs. 6, 7. Regarding G_E^p, G_M^p/μ_p, G_M^n/μ_n, within line width, the data parametrisations are indistinguishable from our predictions – so, not drawn. The parametrisation is drawn in Fig. 7A, making manifest the $\approx 20\%$ underestimate of G_E^n.

It is interesting to observe that, using the meson bound-state analogue of the approach employed herein [42], both the charged ρ- and K^*-meson electric form factors are predicted to exhibit a zero, whereas no zero is predicted in the neutral-K^* form factor. The explanation for the absence of a zero in the neutral-K^* electric form factor [42] is somewhat similar to that presented for G_E^n. Notably, relocating the zero in G_E^ρ by the ratio m_p^2/m_ρ^2, it is placed at $9.4(3)\,\text{GeV}^2$, within the domain defined by Eqs. (5).

In supporting the argument associated with Eq. (7), Fig. 8 is useful.

[1] W. J. Marciano, H. Pagels, Quantum Chromodynamics: A Review, Phys. Rept. 36 (1978) 137.

[2] M. Ablikim, et al., Future Physics Programme of BESIII, Chin. Phys. C 44 (4) (2020) 040001.

[3] D. P. Anderle, et al., Electron-ion collider in China, Front. Phys. (Beijing) 16 (6) (2021) 64701.

[4] R. Abdul Khalek, et al., Science Requirements and Detector Concepts for the Electron-Ion Collider: EIC Yellow Report, Nucl. Phys. A 1026 (2022) 122447.

[5] C. Quintans, The New AMBER Experiment at the CERN SPS, Few Body Syst. 63 (4) (2022) 72.

[6] D. S. Carman, R. W. Gothe, V. I. Mokeev, C. D. Roberts, Nucleon Resonance Electroexcitation Amplitudes and Emergent Hadron Mass, Particles 6 (1) (2023) 416–439.

[7] V. I. Mokeev, P. Achenbach, V. D. Burkert, D. S. Carman, R. W. Gothe, A. N. Hiller Blin, E. L. Isupov, K. Joo, K. Neupane, A. Trivedi, First Results on Nucleon Resonance Electroexcitation Amplitudes from $ep \to e'\pi^+\pi^- p'$ Cross Sections at W = 1.4-1.7 GeV and Q^2 = 2.0-5.0 GeV^2, Phys. Rev. C 108 (2) (2023) 025204.

[8] R. F. Streater, A. S. Wightman, PCT, Spin and Statistics, and All That, Addison-Wesley, Reading, Mass, 3rd edn., 1980.

[9] J. Glimm, A. Jaffee, Quantum Physics. A Functional Point of View, Springer-Verlag, New York, 1981.

[10] K. G. Wilson, Confinement of quarks, Phys. Rev. D 10 (1974) 2445–2459.

[11] Y. Aoki, et al., FLAG Review 2021, Eur. Phys. J. C 82 (10) (2022) 869.

[12] G. Eichmann, H. Sanchis-Alepuz, R. Williams, R. Alkofer, C. S. Fischer, Baryons as relativistic three-quark bound states, Prog. Part. Nucl. Phys. 91 (2016) 1–100.

[13] V. D. Burkert, C. D. Roberts, Roper resonance: Toward a solution to the fifty-year puzzle, Rev. Mod. Phys. 91 (2019) 011003.

[14] D. Binosi, Emergent Hadron Mass in Strong Dynamics, Few Body Syst. 63 (2) (2022) 42.

[15] M. Ding, C. D. Roberts, S. M. Schmidt, Emergence of Hadron Mass and Structure, Particles 6 (1) (2023) 57–120.

[16] M. N. Ferreira, J. Papavassiliou, Gauge Sector Dynamics in QCD, Particles 6 (1) (2023) 312–363.

[17] M. Y. Barabanov, et al., Diquark Correlations in Hadron Physics: Origin, Impact and Evidence, Prog. Part. Nucl. Phys. 116 (2021) 103835.

[18] G. Eichmann, R. Alkofer, A. Krassnigg, D. Nicmorus, Nucleon mass from a covariant three-quark Faddeev equation, Phys. Rev. Lett. 104 (2010) 201601.

[19] G. Eichmann, Nucleon electromagnetic form factors from the covariant Faddeev equation, Phys. Rev. D 84 (2011) 014014.

[20] M. K. Jones, et al., G_{E_p}/G_{M_p} ratio by polarization transfer in $\vec{e}p \to e\vec{p}$, Phys. Rev. Lett. 84 (2000) 1398–1402.

[21] O. Gayou, et al., Measurement of G(E(p))/G(M(p)) in $\vec{e}p \to e\vec{p}$ to Q^2 = 5.6 GeV^2, Phys. Rev. Lett. 88 (2002) 092301.

[22] V. Punjabi, et al., Proton elastic form factor ratios to Q^2 = 3.5 GeV^2 by polarization transfer, Phys. Rev. C 71 (2005) 055202, [Erratum-ibid. C **71**, 069902 (2005)].

[23] A. J. R. Puckett, et al., Recoil Polarization Measurements of the Proton Electromagnetic Form Factor Ratio to Q^2 = 8.5 GeV^2, Phys. Rev. Lett. 104 (2010) 242301.

[24] A. J. R. Puckett, E. J. Brash, O. Gayou, M. K. Jones, L. Pentchev, et al., Final Analysis of Proton Form Factor Ratio Data at Q^2 = 4.0, 4.8 and 5.6 GeV^2, Phys. Rev. C 85 (2012) 045203.

[25] A. J. R. Puckett, et al., Polarization Transfer Observables in Elastic Electron Proton Scattering at Q^2 =2.5, 5.2, 6.8, and 8.5 GeV^2, Phys. Rev. C 96 (2017) 055203, [erratum: Phys. Rev. C **98**, 019907 (2018)].

[26] G. Cates, C. de Jager, S. Riordan, B. Wojtsekhowski, Flavor decomposition of the elastic nucleon electromagnetic form factors, Phys. Rev. Lett. 106 (2011) 252003.

[27] B. Wojtsekhowski, Flavor Decomposition of Nucleon Form Factors – arXiv:2001.02190 [nucl-ex], 2020.

[28] G. Gilfoyle, Future Measurements of the Nucleon Elastic Electromagnetic Form Factors at Jefferson Lab, EPJ Web Conf. 172 (2018) 02004.

[29] H. J. Munczek, Dynamical chiral symmetry breaking, Goldstone's theorem and the consistency of the Schwinger-Dyson and Bethe-Salpeter Equations, Phys. Rev. D 52 (1995) 4736–4740.

[30] A. Bender, C. D. Roberts, L. von Smekal, Goldstone Theorem and Diquark Confinement Beyond Rainbow- Ladder Approximation, Phys. Lett. B 380 (1996) 7–12.

[31] L. Schlessinger, C. Schwartz, Analyticity as a Useful Computation Tool, Phys. Rev. Lett. 16 (1966) 1173–1174.

[32] L. Schlessinger, Use of Analyticity in the Calculation of Nonrelativistic Scattering Amplitudes, Phys. Rev. 167 (1968) 1411–1423.

[33] R. A. Tripolt, I. Haritan, J. Wambach, N. Moiseyev, Threshold energies and poles for hadron physical problems by a model-independent universal algorithm, Phys. Lett. B 774 (2017) 411–416.

[34] Z.-F. Cui, D. Binosi, C. D. Roberts, S. M. Schmidt, Hadron and light nucleus radii from electron scattering, Chin. Phys. C 46 (12) (2022) 122001.

[35] D. Binosi, A. Pilloni, R.-A. Tripolt, Study for a model-independent pole determination of overlapping resonances, Phys. Lett. B 839 (2023) 137809.

[36] Z.-F. Cui, D. Binosi, C. D. Roberts, S. M. Schmidt, D. N. Triantafyllopoulos, Fresh look at experimental evidence for odderon exchange, Phys. Lett. B 839 (2023) 137826.

[37] S.-X. Qin, C. D. Roberts, S. M. Schmidt, Poincaré-covariant analysis of heavy-quark baryons, Phys. Rev. D 97 (2018) 114017.

[38] Q.-W. Wang, S.-X. Qin, C. D. Roberts, S. M. Schmidt, Proton tensor charges from a Poincaré-covariant Faddeev equation, Phys. Rev. D 98 (2018) 054019.

[39] S.-X. Qin, C. D. Roberts, S. M. Schmidt, Spectrum of light- and heavy-baryons, Few Body Syst. 60 (2019) 26.

[40] P. Maris, C. D. Roberts, π and K meson Bethe-Salpeter amplitudes, Phys. Rev. C 56 (1997) 3369–3383.

[41] A. Bashir, A. Raya, S. Sánchez-Madrigal, C. D. Roberts, Gauge invariance of a critical number of flavours in QED3, Few Body Syst. 46 (2009) 229–237.

[42] Y.-Z. Xu, D. Binosi, Z.-F. Cui, B.-L. Li, C. D. Roberts, S.-S. Xu, H.-S. Zong, Elastic electromagnetic form factors of vector mesons, Phys. Rev. D 100 (2019) 114038.

[43] G. Eichmann, C. S. Fischer, Nucleon axial and pseudoscalar form factors from the covariant Faddeev equation, Eur. Phys. J. A 48 (2012) 9.

[44] S.-X. Qin, L. Chang, Y.-X. Liu, C. D. Roberts, D. J. Wilson, Interaction model for the gap equation, Phys. Rev. C 84 (2011) 042202(R).

[45] D. Binosi, L. Chang, J. Papavassiliou, C. D. Roberts, Bridging a gap between continuum-QCD and *ab initio* predictions of hadron observables, Phys. Lett. B 742 (2015) 183–188.

[46] L. Chang, Y.-X. Liu, C. D. Roberts, Y.-M. Shi, W.-M. Sun, H.-S. Zong, Chiral susceptibility and the scalar Ward identity, Phys. Rev. C 79 (2009) 035209.

[47] Z.-N. Xu, Z.-Q. Yao, S.-X. Qin, Z.-F. Cui, C. D. Roberts, Bethe–Salpeter kernel and properties of strange-quark mesons, Eur. Phys. J. A 59 (3) (2023) 39.

[48] Y.-Z. Xu, M. Ding, K. Raya, C. D. Roberts, J. Rodríguez-Quintero, S. M. Schmidt, Pion and kaon electromagnetic and gravitational form factors, Eur. Phys. J. C 84 (2) (2024) 191.

[49] R. L. Workman, et al., Review of Particle Physics, PTEP 2022 (2022) 083C01.

[50] S.-X. Qin, C. D. Roberts, Impressions of the Continuum Bound State Problem in QCD, Chin. Phys. Lett. 37 (12) (2020) 121201.

[51] R. Sachs, High-Energy Behavior of Nucleon Electromagnetic Form Factors, Phys. Rev. 126 (1962) 2256–2260.

[52] P. Maris, P. C. Tandy, QCD modeling of hadron physics, Nucl. Phys. Proc. Suppl. 161 (2006) 136–152, doi: "bibinfodoi10.1016/j.nuclphysbps.2006.08.012.

[53] A. Krassnigg, Excited mesons in a Bethe-Salpeter approach, PoS CONFINEMENT 8 (2008) 075.

[54] P. Maris, P. C. Tandy, The π, K^+, and K^0 electromagnetic form factors, Phys. Rev. C 62 (2000) 055204.

[55] L. Chang, Y.-X. Liu, C. D. Roberts, Dressed-quark anomalous magnetic moments, Phys. Rev. Lett. 106 (2011) 072001.

[56] A. Bashir, R. Bermúdez, L. Chang, C. D. Roberts, Dynamical chiral symmetry breaking and the fermion–gauge-boson vertex, Phys. Rev. C 85 (2012) 045205.

[57] Z.-F. Cui, D. Binosi, C. D. Roberts, S. M. Schmidt, Fresh extraction of the proton charge radius from electron scattering, Phys. Rev. Lett. 127 (9) (2021) 092001.

[58] Z.-F. Cui, D. Binosi, C. D. Roberts, S. M. Schmidt, Pauli radius of the proton, Chin. Phys. Lett. *Express* 38 (12) (2021) 121401.

[59] J. Arrington, W. Melnitchouk, J. A. Tjon, Global analysis of proton elastic form factor data with two-photon exchange corrections, Phys. Rev. C 76 (2007) 035205.

[60] I. Passchier, et al., The Charge form-factor of the neutron from the reaction ^{2}H$(\vec{e}, e'n)p$, Phys. Rev. Lett. 82 (1999) 4988–4991.

[61] C. Herberg, et al., Determination of the neutron electric form-factor in the D$(e, e'n)p$ reaction and the influence of nuclear binding, Eur. Phys. J. A 5 (1999) 131–135.

[62] H. Zhu, et al., A Measurement of the electric form-factor of the neutron through $\vec{d}(\vec{e}, e'n)p$ at $Q^2 = 0.5\,(\text{GeV/c})^2$, Phys. Rev. Lett. 87 (2001) 081801.

[63] J. Bermuth, et al., The Neutron charge form-factor and target analyzing powers from ^{3}He$(\vec{e}, e'n)$ scattering, Phys. Lett. B 564 (2003) 199–204.

[64] G. Warren, et al., Measurement of the electric form-factor of the neutron at $Q^2 = 0.5$ and $1.0\,GeV^2/c^2$, Phys. Rev. Lett. 92 (2004) 042301.

[65] D. Glazier, et al., Measurement of the electric form-factor of the neutron at $Q^2 = 0.3\,(\text{GeV/c})^2$ to $0.8\,(\text{GeV/c})^2$, Eur. Phys. J. A 24 (2005) 101–109.

[66] B. Plaster, et al., Measurements of the neutron electric to magnetic form-factor ratio G_E^n/G_M^n via the ^{2}H$(\vec{e}, e'\vec{n})^1$H reaction to $Q^2 = 1.45\,(\text{GeV/c})^2$, Phys. Rev. C 73 (2006) 025205.

[67] E. Geis, et al., The Charge Form Factor of the Neutron at Low Momentum Transfer from the $^2\vec{\text{H}}(\vec{e}, e'n)p$ Reaction, Phys. Rev. Lett. 101 (2008) 042501.

[68] S. Riordan, S. Abrahamyan, B. Craver, A. Kelleher, A. Kolarkar, et al., Measurements of the Electric Form Factor of the Neutron up to $Q^2 = 3.4 GeV^2$ using the Reaction $^3\vec{\text{He}}(\vec{e}, e'n)pp$, Phys. Rev. Lett. 105 (2010) 262302.

[69] A. Lung, et al., Measurements of the electric and magnetic form-factors of the neutron from $Q^2 = 1.75\,(\text{GeV/c})^2$ to $4\,(\text{GeV/c})^2$, Phys. Rev. Lett. 70 (1993) 718–721.

[70] H. Anklin, et al., Precise measurements of the neutron magnetic form-factor, Phys. Lett. B 428 (1998) 248–253.

[71] G. Kubon, et al., Precise neutron magnetic form-factors, Phys. Lett. B 524 (2002) 26–32.

[72] B. Anderson, et al., Extraction of the Neutron Magnetic Form Factor from Quasi-elastic $^3\vec{He}(\vec{e}, e')$ at Q^2 = 0.1 - 0.6 (GeV/c)^2, Phys. Rev. C 75 (2007) 034003.

[73] J. Lachniet, et al., A Precise Measurement of the Neutron Magnetic Form Factor G_M^n in the few-GeV^2 Region, Phys. Rev. Lett. 102 (2009) 192001.

[74] J. Segovia, I. C. Cloet, C. D. Roberts, S. M. Schmidt, Nucleon and Δ elastic and transition form factors, Few Body Syst. 55 (2014) 1185–1222.

[75] D. J. Wilson, I. C. Cloet, L. Chang, C. D. Roberts, Nucleon and Roper electromagnetic elastic and transition form factors, Phys. Rev. C 85 (2012) 025205.

[76] I. C. Cloet, C. D. Roberts, A. W. Thomas, Revealing dressed-quarks via the proton's charge distribution, Phys. Rev. Lett. 111 (2013) 101803.

[77] R. Madey, et al., Measurements of G_E^n/G_M^n from the ^{2}H$(\vec{e}, e'\vec{n})$ reaction to $Q^2 = 1.45\,(\text{GeV}/c)^2$, Phys. Rev. Lett. 91 (2003) 122002.

[78] Z.-F. Cui, C. Chen, D. Binosi, F. de Soto, C. D. Roberts, J. Rodríguez-Quintero, S. M. Schmidt, J. Segovia, Nucleon elastic form factors at accessible large spacelike momenta, Phys. Rev. D 102 (2020) 014043.

[79] P. E. Shanahan, R. Horsley, Y. Nakamura, D. Pleiter, P. E. L. Rakow, G. Schierholz, H. Stüben, A. W. Thomas, R. D. Young, J. M. Zanotti, Determination of the strange nucleon form factors, Phys. Rev. Lett. 114 (2015) 091802.

[80] I. C. Cloet, C. D. Roberts, Explanation and Prediction of Observables using Continuum Strong QCD, Prog. Part. Nucl. Phys. 77 (2014) 1–69.

[81] C. Kallidonis, et al., Nucleon electromagnetic form factors at high Q^2 from Wilson-clover fermions, PoS LATTICE2018 (2018) 125.

[82] G. Eichmann, C. S. Fischer, W. Heupel, N. Santowsky, P. C. Wallbott, Four-quark states from functional methods, Few Body Syst. 61 (2020) 38.

[83] C. D. Roberts, D. G. Richards, T. Horn, L. Chang, Insights into the emergence of mass from studies of pion and kaon structure, Prog. Part. Nucl. Phys. 120 (2021) 103883.

[84] J. J. Kelly, Simple parametrization of nucleon form factors, Phys. Rev. C 70 (2004) 068202.

[85] Z.-F. Cui, J.-L. Zhang, D. Binosi, F. de Soto, C. Mezrag, J. Papavassiliou, C. D. Roberts, J. Rodríguez-Quintero, J. Segovia, S. Zafeiropoulos, Effective charge from lattice QCD, Chin. Phys. C 44 (2020) 083102.

[86] A. Deur, S. J. Brodsky, C. D. Roberts, QCD Running Couplings and Effective Charges, Prog. Part. Nucl. Phys. 134 (2024) 104081.